Equivalent Annular Model of a Multitubular Shell-Side (MSS) Fixed-Bed Reactor

Haoming Li, Robert R. Hudgins, and Kun Soo Chang
Dept. of Chemical Engineering, University of Waterloo, Waterloo, Ontario, Canada N2L 3G1

For a multitube catalytic reactor in which catalyst occupies the shell side of the cooling tubes, a two-dimensional model is developed to determine the nonuniform radial distribution of the temperature and concentration. The cross-section of the fixed bed is divided into a number of equivalent portions proportional to the number of cooling tubes. Each portion is approximated by either an equivalent annular fixed bed or a transformed circular fixed bed in the complex plane. Enthalpy and mass balances are performed on the equivalent annular fixed bed while the radially varying flow distribution and the transport properties are considered in a transformed circular fixed bed. A correlation is developed for the equivalent annular model based on the relationship of the two different approximations. The model can also account for variations in radial porosity, radial velocity, and transport properties.

Introduction

The behavior of industrial reactors can be influenced, often greatly, by radial gradients in the porosity of the bed, the fluid velocity, the temperature, and so on. For example, radial variations in temperature can make a reactor unstable, given certain inherent fluctuations in some of its operating variables (Leron and Froment, 1977). Also in activating a commercial catalyst, an uneven distribution of temperature can cause incomplete reduction and possibly rapid deterioration of the catalyst activity. During day-to-day operation of a catalytic reactor, severe radial temperature gradients can impair the activity of the catalyst and shorten its life. Therefore, it is our purpose to study how radial variations of the flow rate and of the transport properties affect the behavior of a reactor. Previous studies of radial temperature gradients in reactors, whether with plug flow or nonplug flow, have dealt with single-tube fixed-bed reactors (Ahmed and Fahien, 1980; Touzani et al., 1987), whereas modeling of a multitubular shell-side (MSS) fixed-bed reactor has been restricted to the assumption of plug flow (Hlavacek and Votruba, 1977).

An MSS fixed-bed reactor is a modification of a shell-and-tube heat exchanger consisting of arrays of small-diameter tubes in which catalyst pellets occupy the free volume on the shell side. The feed stream flows through the tube-side where it can be preheated before entering the packed bed. This type of reactor is commonly used in the industrial manufacture of ammonia (Strelzoff, 1981). Figure 1 is a schematic of the particular industrial ammonia synthesis reactor modeled in this paper. Plant data from this reactor were recorded by Li (1982). The reactor consists of an adiabatic section followed by an MSS cooling section. As shown in Figure 1a, the cold feed stream, containing both hydrogen and nitrogen in stoichiometric proportion, reaches the top of the parallel cooling tubes through two side ducts. As a coolant, it flows concurrently through a number of cooling tubes and is preheated to its desired reaction temperature. It then enters the fixed bed from the top of the adiabatic section and flows downward through the iron catalyst on the shell-side of the cooling section. Much of the heat generated in the bed is transmitted to the coolant-feed; thus, the reactor operates autothermally. Even though the reaction in the adiabatic section rapidly raises the temperature close to the optimum value, heat transfer through the cooling tubes prevents the catalyst from being overheated while keeping the conversion in the optimum region. Figure 1b is a view of the cross section of the cooling section. The fraction of catalyst cooled by each cooling tube is about the same. One way to model a reactor of this type is by means of a three-variable, two-dimensional plug-flow model approximating the shell-side configuration as shown in Figure 2a. Such a model was developed by Hlavacek and Votruba (1977).

Correspondence concerning this article should be addressed to K. S. Chang who is presently with the POSTECH, Pohang Institute of Science and Technology, P.O. Box 125, Pohang, 790-600 Korea.
Present address of H. Li: Canadian Fertilizers, P.O. Box 1300, Medicine Hat, Alberta, Canada, T1A 7R9.

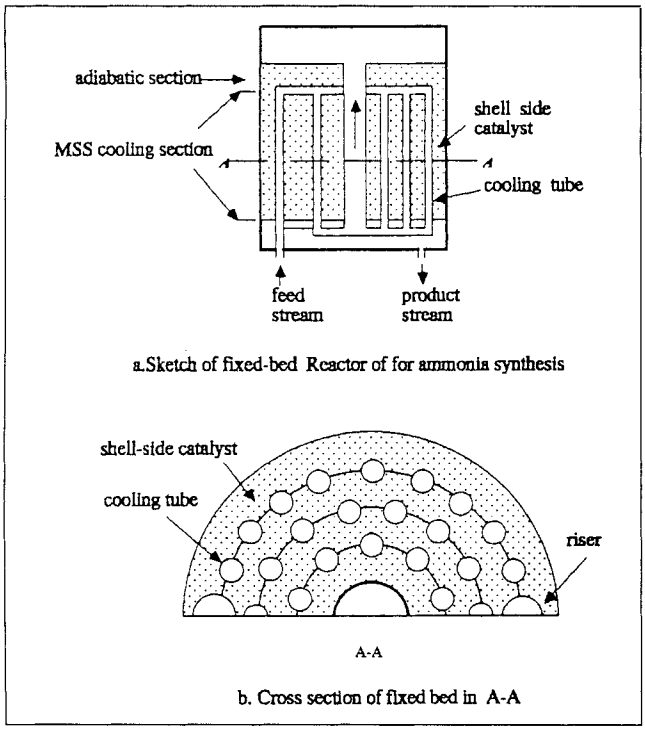

Figure 1. Typical multitubular shell-side packed bed for ammonia synthesis.

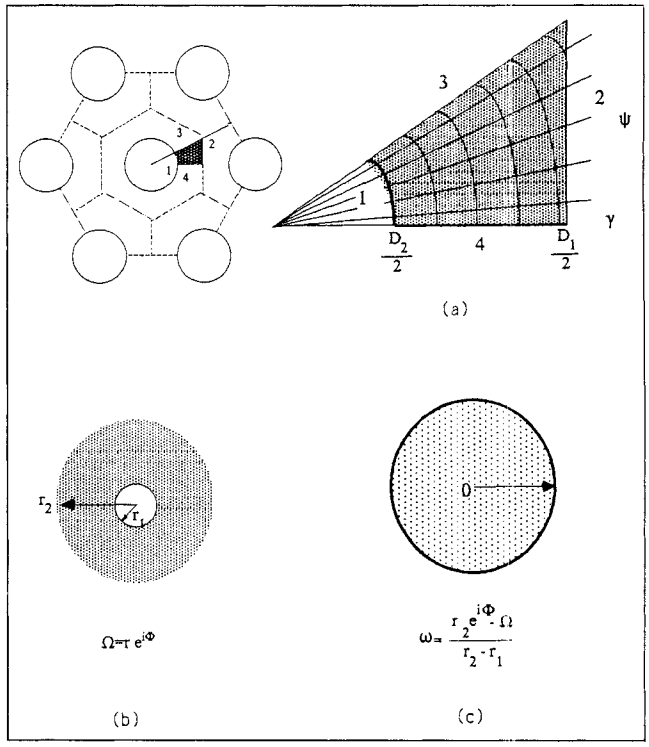

Figure 2. Different approximations of shell-side fixed bed.

(a) for three-variable model showing 1/12 of the hexagonal area
(b) equivalent annular model with area equal to that of a hexagon
(c) transformed circular model with area equal to that of a hexagon

In this article, a new semi-two-dimensional model (i.e., two-dimensional with respect to temperature, but one-dimensional with respect to mole fraction) is developed and correlations for flow rate and transport properties are introduced for the complex geometry of the catalyst packing in a multitubular shell-side reactor in order to calculate the effect of radial non-uniformity of porosity, velocity and transport properties on its performance.

Equivalent Annular Pattern and Transformed Circular Pattern

The challenge in modeling an MSS fixed-bed reactor is how to handle the irregularity of the boundary of the shell-side packing. There are different ways of approximating this configuration. One such method, already mentioned, is suggested by Figure 2a. The cross-section of the reactor bed of Figure 1b is considered to be subdivided into identical hexagonal areas centered about each cooling tube. These hexagonal elements pack into a hexagonal matrix of cooling tubes surrounded by catalyst packing. In the present analysis, we first approximate the entire multitubular shell-side packing with an equivalent annular pattern (Figure 2b) instead of the hexagon used by Hlavacek and Votruba, and refer to it as an equivalent annular (EA) model. The outer and inner diameters of the annular boundary are:

$$d_2 = \sqrt{\frac{d_{\text{bed}}^2 - d_{\text{c.t}}^2 - 2d_{\text{riser}}^2}{m_t}} \tag{1}$$

$$d_1 = d_a \tag{2}$$

where

d_{bed} = diameter of the packed bed
$d_{c.t}$ = diameter of central tube
d_{riser} = diameter of the side risers
d_a = diameter of a cooling tube
m_t = number of cooling tubes

The cross area of an equivalent annulus can be represented as:

$$\Omega = re^{i\Phi} \quad (r_1 \le r \le r_2) \tag{3}$$

where $r = r_1$ is for the tube wall and $r = r_2$ is the central position of shell-side packings.

A material balance on the product and an energy balance across the fixed bed yields a two-dimensional model for this equivalent annular configuration:

$$\frac{\partial [uc]}{\partial x} = \frac{1}{r}\frac{\partial}{\partial r}\left(D_r r \frac{\partial c}{\partial r}\right) + r(T,c) \tag{4}$$

$$\rho u \bar{c}_p \frac{\partial T}{\partial x} = \frac{1}{r}\frac{\partial}{\partial r}\left(k_{er} r \frac{\partial T}{\partial r}\right) + (-\Delta H) r(T,c) \tag{5}$$

with boundary conditions

$$x = 0,\ r_1 \le r \le r_2;\ T = T_{\text{inlet}},\ c = c_{\text{inlet}};$$

$$r = r_1,\ 0 \le x \le L;\ \frac{\partial c}{\partial r} = 0,\ k_{er}\frac{\partial T}{\partial r} = k_{wf}(T_r - T_c);$$

$$r = r_2,\ 0 < x \le L;\ \frac{\partial c}{\partial r} = 0,\ \frac{\partial T}{\partial r} = 0$$

Alternatively, the shell-side fixed bed can be regarded as an area surrounded by tube walls; this area can be approximated by a number of transformed circular fixed beds transformed into the complex plane:

$$\omega = r_2 e^{i\Phi} - \Omega \tag{6a}$$

or its normalized form

$$\omega = \frac{r_2 e^{i\Phi} - \Omega}{r_2 - r_1}. \tag{6b}$$

The behavior of the catalyst at any point bounded by the catalytic bed and the cooling tube wall (i.e., on the shell side) can be considered as having a counterpart lying within an equivalent annulus (Figure 2b) or between a transformed circle center and its circumference respectively. The latter model is referred to as an "imaginary fixed bed" with the subscript "im" (Figure 2c) later in this paper. We also refer to it as the "transformed circular model." The normal radial position is $\gamma_{im} = (r_2 - r)/(r_2 - r_1)$. In the complex plane ($\gamma_{im}$, ϕ), Eq. 6b provides the analytical description of each element of the complex configuration. Because points having the same radial coordinate behave identically, we can thus examine radial variations of temperature and concentration within the complex geometry of the MSS reactor. The dimensionless diameters of the pellets, $d_p/(r_2 - r_1)$, calculated using either equivalent annular or transformed circular geometries, are identical. However, the local void volume is a function of the distance from the tube wall measured in terms of the number of catalyst pellet diameters, as follows:

$$\epsilon_{im} = f\left(\frac{0.5D_t - r}{d_p}\right)_{im} = f\left(\frac{0.5(D_2 - D_1) - (r_2 - r)}{d_p}\right) = \epsilon. \tag{7}$$

Thus, we have the same description of both the pellet array and the radial variation of the voidage by either model.

A comparison of the two geometric configuration approximations provides the following relationship:

$$\gamma_{im} = \frac{r_2 - r}{r_2 - r_1} = 1 - \gamma, \quad \left(\gamma = \frac{r - r_1}{r_2 - r_1}\right). \tag{8}$$

The heat exchanger tubes are packed in a hexagonal array that can be depicted by drawing around the circular tubes identical symmetrical hexagons, as in Figure 2. This hexagonal boundary around each tube maps onto the center of the transformed circular fixed bed, while the tube wall maps onto the transformed circle. Thus, the quantities of syngas passing through each cross-sectional position in the transformed geometry must be weighted. For this purpose, we now develop a weighting function for the flow rate.

Flow Distribution Across the Bed (on the Shell-Side)

Fahien and Stankovich (1979) represents the dimensionless flow rate in terms of the pellet diameter, and tube radius, and the dimensionless radial position. Ahmed and Fahien (1980) and Touzani et al. (1987) applied it in a two-dimensional model of a tubular reactor. If we apply their correlation in the imaginary fixed bed, the velocity expression for the shell-side fixed bed can be written as:

$$v_{im} = \frac{1}{2D}\left(A_1 + A_2\gamma_{im}^{b+1} - A_3\gamma_{im}^{b+2}\right) \tag{9}$$

where

$$A_1 = \frac{1}{b+2} - \frac{[\gamma_m]_{im}}{b+1}$$

$$b = 0.16\alpha_{im}^{-\frac{3}{2}}, \quad \alpha_{im} = \left(\frac{d_p}{D_t}\right)_{im}, \quad [\gamma_m]_{im} = 1 - 2\alpha_{im}$$

$$A_2 = \frac{[\gamma_m]_{im}}{b+1}, \quad A_3 = \frac{1}{b+2}.$$

The normal pellet size and the normal radial coordinate can be deduced from Eq. 6. We can write the average flow rate in the equivalent annular geometric configuration as follows:

$$u_{av} = \frac{\int_{r_1}^{r_2} urdr}{\int_{r_1}^{r_2} rdr}.$$

For the transformed circular geometric configuration we can determine the constant $2D$ for the shell-side packed bed from previous studies.

$$(v_{av})_{im} = \frac{\int_0^1 v_{im}(1 - \gamma_{im})d\gamma_{im}}{\int_0^1 (1 - \gamma_{im})d\gamma_{im}} = 1. \tag{10}$$

By substituting the expression for v from Eq. 9 into Eq. 10, the following formula for $2D$ is obtained:

$$\frac{1}{2D} = \frac{1}{A_1 - 2A_2\frac{1}{b+3} + 2A_2\frac{1}{b+2} + 2A_3\frac{1}{b+4} - 2A_3\frac{1}{b+3}}. \tag{11}$$

From the heat transfer model of Yagi and Wakao (1959), we have the following expression for the effective thermal conductivity (Yagi and Kunii, 1957):

$$\frac{k_{er}}{\lambda_f} = \frac{k_{eo}}{\lambda_f} + \alpha_1\alpha_2\, Re_p\, Pr. \tag{12}$$

The bed-coolant heat transfer coefficient is written as:

$$k_{wf} = \frac{1}{\frac{D_m}{\alpha_w D_w} + \frac{D_m}{\alpha_f D_i} + \frac{\delta}{\lambda_{tu}} + Rc} \tag{13}$$

where α_f is the wall-to-coolant heat transfer coefficient given by the formula:

$$\alpha_f = 0.023 \frac{\lambda_f}{De} Re^{0.8} Pr^{0.3}.$$

The radial dispersion coefficient is given as (Smith, 1981):

$$D_r = \frac{d_p u}{Pe_m}. \tag{14}$$

Rather than using average values for the mean flow and mean voidage in Eqs. 12 through 14, we incorporate these relations and the velocity correlation in Eq. 9. They provide point values of each parameter across the radius of the bed for the model equations (Eqs. 4 and 5).

Solution of the EA Model by the Method of Orthogonal Collocation

Because of the highly nonlinear nature of the reaction rate, we have to resort to numerical methods to solve Eqs. 4 and 5. These coupled partial differential equations can be converted into a system of simultaneous first-order ordinary differential equations by the method of orthogonal collocation (Finlayson, 1972, 1977).

We define a normalized radius as follows:

$$\xi = \frac{r - r_1}{r_2 - r_1}. \tag{15}$$

The collocation points are given by the roots of the orthogonal polynomials:

$$P_i(\xi) = 1 + \frac{(-i)\left(i + \frac{a}{2} + 1\right)}{2 \cdot 1! \left(\frac{a}{2}\right)} \xi + \ldots + \frac{(-i)(-i+1)\ldots(-1)\left(i+\frac{a}{2}+1\right)\ldots\left(i+\frac{a}{2}+i\right)}{(i+1)i!\left(\frac{a}{2}\right)\left(\frac{a}{2}+1\right)\ldots\left(\frac{a}{2}+i-1\right)} \xi^i \tag{16}$$

and the point temperature at the collocation points can be expressed as:

$$T_i(\xi) = \sum_{j=1}^{N+2} d_j \xi_i^{j-1} \tag{17}$$

$dT/d\xi$ and $d^2T/d\xi^2$ may be expressed in terms of the values of $T(\xi_i)$ in the collocation points $\xi_1, \xi_2, \ldots \xi_{N+2}$ ($\xi_1 = 0$, $\xi_{N+2} = 1$). In matrix notation, we write

$$[T_i] = [\xi_i^{j-1}][d_j] = \boldsymbol{CD} \tag{18}$$

$$\left[\frac{dT_i}{d\xi}\right] = [(j-1)\xi_i^{j-2}][d_j] = \boldsymbol{AD} \tag{19}$$

$$\left[\frac{d^2T_i}{d\xi^2}\right] = [(j-1)(j-2)\xi_i^{j-3}][d_j] = \boldsymbol{BD}. \tag{20}$$

Solving for $\boldsymbol{D}$ in Eq. 18 to get $\boldsymbol{D} = (\boldsymbol{C}^T\boldsymbol{C})^{-1}\boldsymbol{C}^T\boldsymbol{T}$, we have:

$$\frac{dT}{d\xi} = A(\boldsymbol{C}^T\boldsymbol{C})^{-1}\boldsymbol{C}^T\boldsymbol{T} = \boldsymbol{FT} \tag{21}$$

$$\frac{d^2T}{d\xi^2} = \boldsymbol{B}(\boldsymbol{C}^T\boldsymbol{C})^{-1}\boldsymbol{C}^T\boldsymbol{T} = \boldsymbol{GT}. \tag{22}$$

Combining the temperature derivatives with Eq. 15, we obtain:

$$\frac{\partial T_i}{\partial r} = \frac{1}{r_2 - r_1}\frac{\partial T_i}{\partial \xi} = \frac{1}{r_2 - r_1}\sum_{j=1}^{N+2} F_{ij} T_{j-1} \tag{23}$$

and

$$\frac{\partial^2 T_i}{\partial r^2} = \frac{1}{(r_2 - r_1)^2}\frac{\partial^2 T_i}{\partial \xi^2} = \frac{1}{(r_2 - r_1)^2}\sum_{j=1}^{N+2} G_{ij} T_{j-1}. \tag{24}$$

For the concentration c, the same formulation applies and similar equations can be written.

Application to an Ammonia Synthesis Reactor

The validity of the multitubular model expressed by Eqs. 4 and 5 can be tested by comparing the theoretical predictions obtained from the model with plant data from an industrial ammonia synthesis reactor. The following analysis of the ammonia synthesis reaction based on N_o kmol of synthesis gases (N_2 and H_2) provides the relationship between the reactants and the product during the reaction. When X kmol of ammonia are produced, $N_o - 2X$ kmol of synthesis gas remain unreacted. Thus, along the axial direction of the fixed bed, the gas flux ($N_z = N_o - X$) is not equimolar. At any axial position z in the bed where the mole fraction ammonia concentration is $y_a = X/(N_o - X)$, the molar flux is:

$$N_z = \frac{N_o}{1 + y_a}. \tag{25}$$

Expressing the ammonia concentration as a mole fraction instead of a molar concentration c in Eqs. 4 and 5, we obtain:

$$uc = N_z y. \tag{26}$$

Substitution of Eqs. 25 and 26 in Eqs. 4 and 5 generates a model for a tubular ammonia synthesis reactor:

$$\frac{\partial y}{\partial x} = \frac{1+y}{u}\left\{\frac{D_r}{r}\frac{\partial y}{\partial r} + \frac{\partial}{\partial r}\left(D_r \frac{\partial y}{\partial r}\right)\right\} + \frac{1}{w} r(y,T) \tag{27}$$

$$\frac{\partial T}{\partial x} = \frac{M_{av}}{G\bar{c}_p}\left\{\frac{k_{er}}{r}\frac{\partial T}{\partial r} + \frac{\partial}{\partial r}\left(k_{er}\frac{\partial T}{\partial r}\right)\right\} + \frac{(-\Delta H)}{Gc_p(1+y)^2} r(y,T) \tag{28}$$

subject to the boundary conditions:

$$x = 0,\ r_1 \le r \le r_2;\ T = T_{\text{inlet}},\ y = y_{\text{inlet}}$$

$$r = r_1,\ 0 \le x \le L;\ \frac{\partial y}{\partial r} = 0,\ k_{er}\frac{\partial T}{\partial r} = k_{wf}(T_w - T_c)$$

$$r=r_2,\ 0\le x\le L;\ \frac{\partial y}{\partial r}=0,\ \frac{\partial T}{\partial r}=0.$$

The reaction rate is a function of operation temperature, pressure and concentrations of all the reactants:

$$r(y,T)=k_T(1+y_a)^2F_a\ (\mathrm{s}^{-1}) \tag{29}$$

where F_a can be calculated by the generally accepted Temkin equation for small particles of catalyst (Rase, 1977):

$$F_a=\left\{\frac{K_p^2P^2\left[y_{H,o}(1+y_a)-\frac{3}{2}y_a\right]^{1.5}\left[y_{N,o}(1+y_a)-\frac{1}{2}y_a\right]}{y_a}-\frac{y_a}{\left[y_{H,o}(1+y_a)-\frac{3}{2}y_a\right]^{1.5}}\right\}P^{-0.5}\left(\frac{3}{4}\right)^{1.5}.$$

The equilibrium constant can be expressed in terms of the partial pressure of hydrogen, nitrogen and ammonia:

$$K_p=\frac{P_a}{P_N^{0.5}P_H^{1.5}}\ (\mathrm{atm}^{-1})$$

and correlated with temperature by the Larson and Dodge empirical equation (Strelzoff, 1981):

$$\mathrm{Log}\ \frac{1}{K_p}=-\frac{2{,}074}{T}+2.4943\ \mathrm{Log}\ T+12.56\times10^{-5}-1.8564\times10^{-7}T^2-2.206 \tag{30}$$

where T is Kelvin temperature. The heat of reaction by the formula of Gillespie and Beattrie (Strelzoff, 1987):

$$\Delta H=\left\{-\left[0.54526+\frac{846.609}{T}+\frac{459.734\times10^6}{T^3}\right]P-5.34685T-0.2525\times10^{-3}T^2+1.69197\times10^{-6}T^3-9{,}157.09\right\}\times4.184\times10^{-3}(\mathrm{kJ/mol}) \tag{31}$$

The reaction rate expression, Eq. 29, is written for small catalyst pellet diameters (say, of the order of 1 mm). This expression must be modified to account for the inter- and intraparticle transport limitations that can occur using larger pellet diameters. At the same time, using larger catalyst pellets can lead to incomplete reduction of the catalyst bed and affect its initial activity. In practice, all such modifications to the reaction constant are combined into a single coefficient having the form $f=f_1-f_2x$. Additional corrections must be made to account for radial variations of the porosity. The superficial reaction rate (Eq. 29) can thus be written in the form of a Temkin equation:

$$r_i(y,T)=\frac{1-\epsilon_i}{1-\epsilon_b}\,r(y,T) \tag{32}$$

where ϵ_b is the bulk density of catalyst for which the rate constant is known. In this study, we have made use of the two-zone assumption of McGreavy et al. (1986) in which there is a region of constant bulk density and a region of variable bulk density decreasing to ϵ_i at the wall.

At the internal collocation points, a set of simultaneous ordinary differential equations generated from the transformed model can be written as:

$$\frac{\partial y_i}{\partial x}=\frac{(1+y_i)d_p}{Pe_i}\times\left\{\left(\frac{1}{r_i}+\frac{1}{u_i}\frac{\partial u_i}{\partial r}\right)\frac{1}{r_2-r_1}\sum_{j=1}^{N+2}F_{ij}y_{j-1}+\frac{1}{(r_2-r_1)^2}\sum_{j=1}^{N+2}G_{ij}y_{j-1}\right\}+\frac{1}{w_i}r(y_i,T_i) \tag{33}$$

$$\frac{\partial T_i}{\partial x}=\frac{22.4k_{er,i}(1+y_i)}{w_i\bar{c}_p}\times\left\{\left(\frac{1}{r_i}+\frac{1}{k_{er,i}}\frac{\partial k_{er,i}}{\partial r}\right)\frac{1}{r_2-r_1}\sum_{j=1}^{N+2}F_{ij}T_{j-1}+\frac{1}{(r_2-r_1)^2}\sum_{j=1}^{N+2}G_{ij}T_{j-1}\right\}+\frac{(-\Delta H)}{w_i\bar{c}_p(1+y_i)}r(y_i,T_i). \tag{34}$$

In view of the boundary conditions at the tube wall in Eqs. 27 and 28 (where $\gamma=0$ or $r=r_1$), we see that

$$\sum_{j=1}^{N+2}F_{1j}y_{j-1}=0 \tag{35}$$

and

$$\frac{k_{er,o}}{r_2-r_1}\sum_{j=1}^{N+2}F_{1j}T_{j-1}=k_{wf}(T_w-T_c). \tag{36}$$

At the center of the shell-side packing where $\gamma=1$ or $r=r_2$, we have

$$\sum_{j=1}^{N+2}F_{N+2,j}y_{j-1}=0 \tag{37}$$

and

$$\sum_{j=1}^{N+2}F_{N+2,j}T_{j-1}=0. \tag{38}$$

Inside each of the cooling tubes, we also have

$$\frac{dT_c}{dx}=\frac{k_{wf}m_t\pi D_m}{N_z\bar{c}_f}\,(T_w-T_c). \tag{39}$$

Results and Discussion

The numerical solutions converge after $N=5$ (number of collocation points = 7) and a step size $\delta x=0.002$. To test the

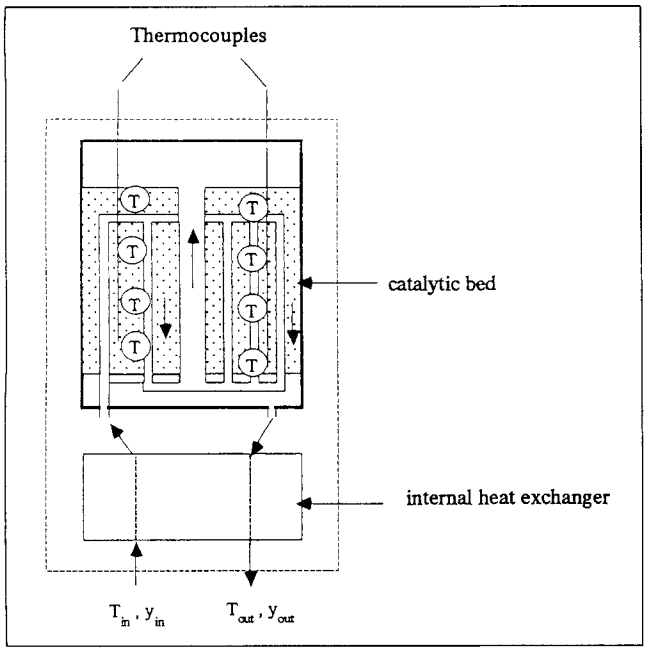

Figure 3. Data collection from MSS ammonia synthesis reactor.

T = thermocouple station

models, we compare predictions obtained by solving Eqs. 33 through 39 with experimental data obtained in the operation of the ammonia synthesis reactor of Figure 1. The operating conditions and the estimated parameters for this reactor are presented in the Appendix. Figure 3 indicates the locations at which the plant thermocouple measurements were taken. These include the axial temperature measurements along the bed length, the adiabatic temperature rise for a given feed composition, and inlet temperature. From feed and effluent concentration measurements, the production capacity was determined for a given set of feed conditions.

At any axial position, the numerical solution of the EA model gives the radial temperature distribution. The average radial temperature is calculated from this distribution to be:

$$u_{av} = \frac{\int_{r_1}^{r_2} Turdr}{\int_{r_1}^{r_2} urdr} = \frac{\int_{r_1}^{r_2} Turdr}{u_{av}\int_{r_1}^{r_2} rdr} = \frac{2}{r_2^2 - r_1^2}\int_{r_1}^{r_2} Tvrdr \qquad (40)$$

where $v = u/u_{av}$ represents the dimensionless point-value of the flow rate at point r.

Various combinations of constant or variable flow distribution and heat transfer were considered, as follows:

Model	Main Features
EA-1	non-PF + nonuniform k_{er} (Figure 4)
EA-2	non-PF + uniform k_{er}
EA-3	PF + uniform k_{er}

In Figure 5, data from actual plant ammonia production are compared with those predicted by the three variants of the

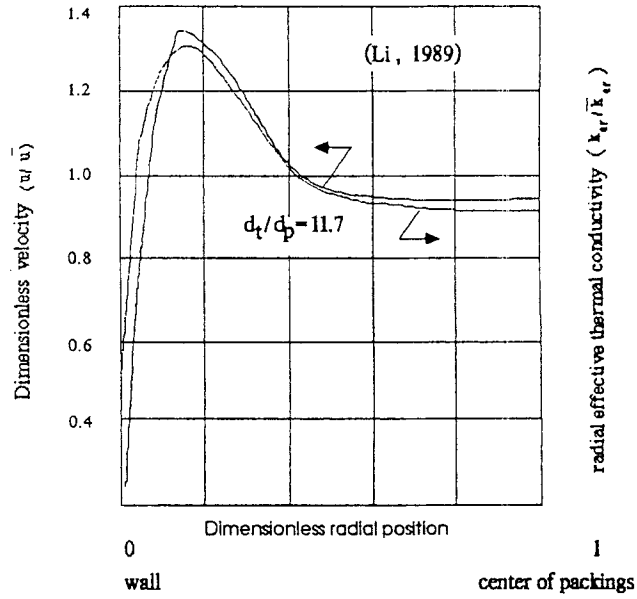

Figure 4. Radial variations in transport properties in the MSS packings.

EA model. The models are generally satisfactory. However, all of the models overestimate the ammonia production by up to about 5 to 7%. This discrepancy is likely due to the neglect of the purge stream used to prevent argon buildup in the full-scale reactor. For present purposes, the rate of ammonia production is based only on a reactor with a single inlet and single exit. We will return to this matter further on.

Only model EA-1 considers variations in the radial effective thermal conductivity. Figure 4 shows this variation to be over a large range near the wall, becoming constant in the region near the center of the catalyst packing. The variation in k_{er} is accounted for by means of the function:

$$k_{er} = f(Re_p, Pr)$$

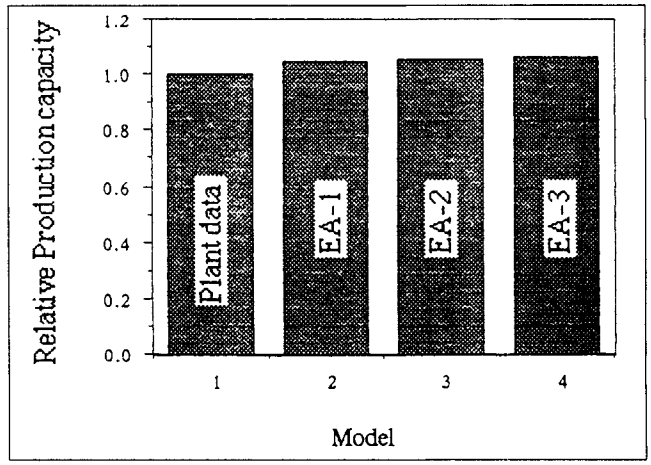

Figure 5. Comparison of production capacities from different models.

Plant data = 10.25 (t/8 h)
model EA-1 = 10.761
EA-2 = 10.817
EA-3 = 10.929

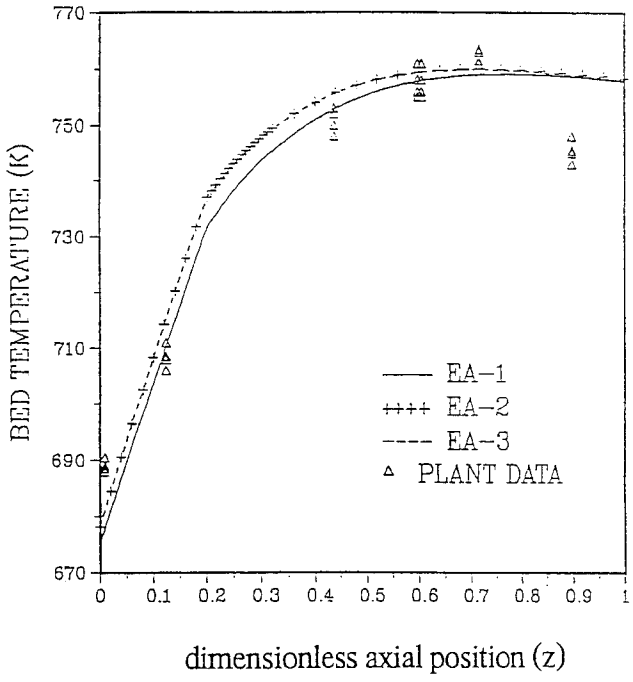

Figure 6. Averaged axial temperature profiles by different models.

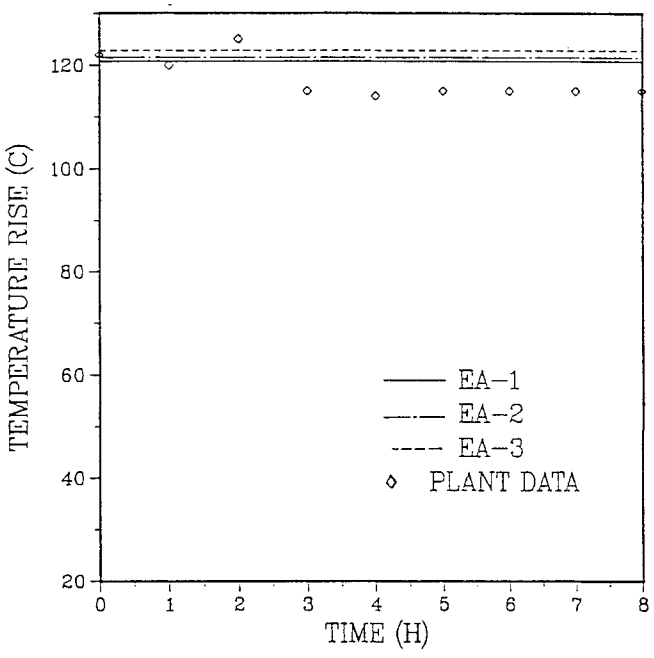

Figure 8. Adiabatic temperature rise by different models.

where point values of Re_p and Pr are used instead of the average values.

Figure 6 shows the predicted averaged axial temperature profiles for the three EA models as well as the plant temperature profiles. Several observations are worthy of note. First of all, the EA models, despite apparent differences, predict rather similar axial temperature profiles. Agreement with the plant temperature profiles along the bed in the range $0.1<z<0.8$ is within about 3°C of the model predictions. Sizable discrepancies of about 10°C occur near the outlet of the fixed bed. These may reflect an overestimation of the catalyst activity in the last section of the reactor because of the failure to estimate an accurate coefficient for the synthesis reaction constant. It is to be noted that axial bed temperatures were measured by means of a thermocouple enclosed within a sheath. The sheath may not have been placed at the precise point in the bed at which the mean temperature occurred. Furthermore, the insertion of such a tube would create its own radial variations in porosity and flow within the packing, so it might not register the "true" temperature of the catalyst bed within the tube array. However, the similarity of the predicted and measured values in Figure 7 (except near the end of the bed) does suggest that the measured temperatures are close to the temperature of the packing.

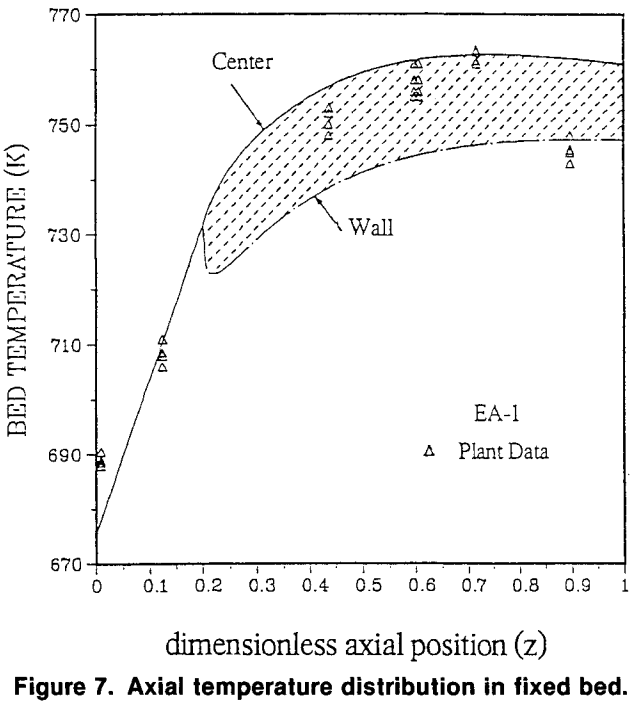

Figure 7. Axial temperature distribution in fixed bed.

In Figure 7, axial temperatures are predicted in the central region of the catalyst packing and at the wall by the EA-1 model. It can be seen that the feed temperature is poorly estimated. In practice, after a period of operation, a certain amount of settling of the catalyst bed may occur. If this is not accounted for in the modeling, the simulated inlet temperature may be a little lower than the experimental value. Also, the temperature at $z=0.9$ is overestimated for reasons already stated. The predictions for center-bed and wall temperatures bracket the measured temperatures in the downstream half of the bed. The adiabatic temperature rise is estimated from an enthalpy balance between the inlet and the outlet streams as follows. If X kmol ammonia are generated from 100 kmol of feed stream, the expected adiabatic temperature rise between the inlet and the outlet of the reactor is:

$$\Delta T=\frac{X\Delta H}{\sum C_{p,i}(100-X)}. \tag{41}$$

When the inlet temperature is given, the exit temperature is predicted from the equation:

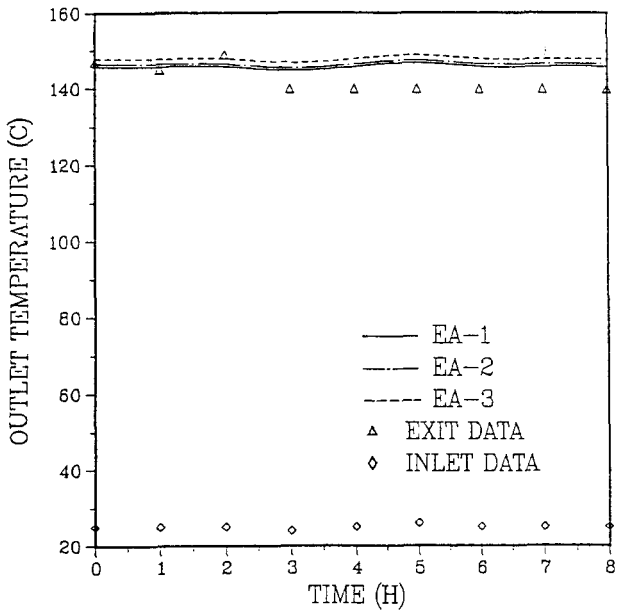

Figure 9. Exit temperatures by different models.

$$T_{\text{exit}} = T_{\text{in}} + \frac{X\Delta H}{\sum C_{p,i}(100 - X)}$$

where $\Sigma C_{p,i}$ is the average heat capacity of the resultant mixture between the inlet and the outlet temperatures, ΔH is the reaction heat at the inlet temperature, and ΔT is the adiabatic temperature rise. This is done in Figure 8. The three variants of the EA model predict adiabatic temperatures within 2°C of one another. Considering that a heat loss of about 5 to 10% occurs in practice, these predictions coincide satisfactorily with the experimental reactor data.

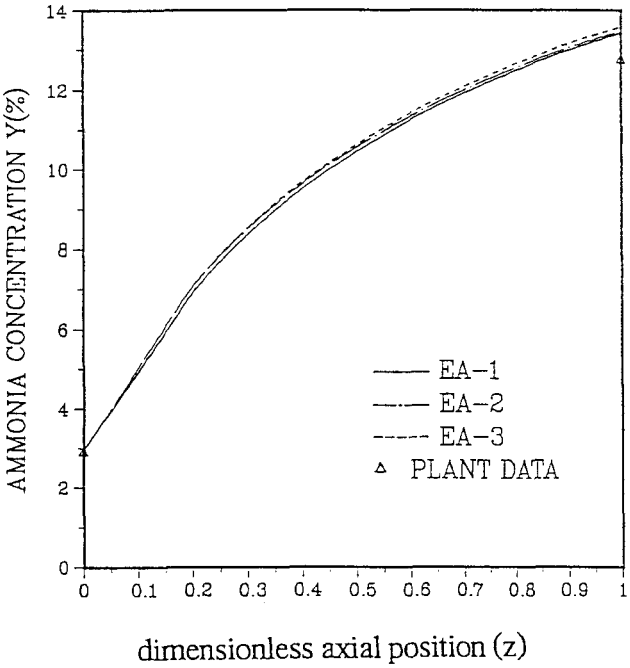

Figure 10. Axial concentration profiles by different models.

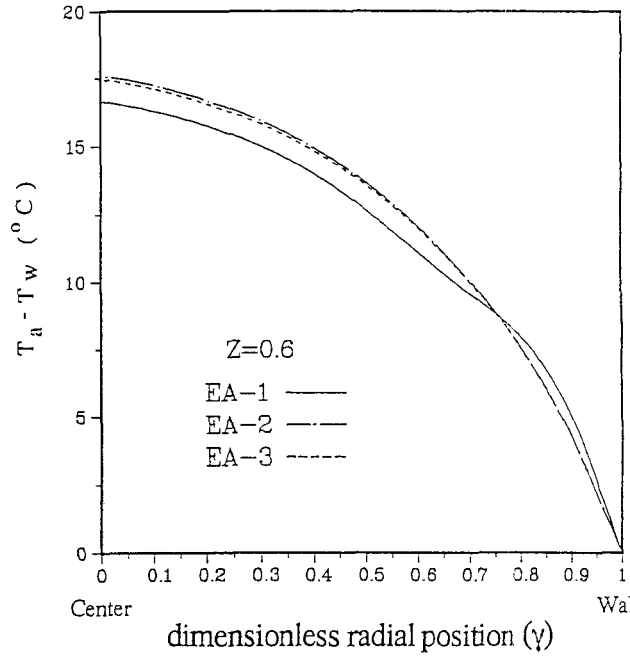

Figure 11. Radial temperature profiles by different models.

Starting from the feed conditions to the fixed bed, we can predict the progress of ammonia synthesis in the reactor, as shown in Figure 9. Based on 100 kmol feed, the production rate is:

$$X = \frac{y_{\text{out}} - y_{\text{in}}}{100 + y_{\text{out}}} \times 100 \text{ (kmol)}. \tag{42}$$

A small amount of purge from the synthesis system appears to cause the overestimation of production capacity. This purge permits inert gases not to accumulate in the synthesis loop beyond some maximum concentration. Suppose the methane in the supplied refinery stream is $y_{CH_{4,1}}$ and in the recycling stream is $y_{CH_{4,2}}$ while the amount of purge is G_p and the supplied feed is G_f. Since

$$y_{CH_{4,1}} G_f = y_{CH_{4,2}} G_p$$

the reduced production because of the purge is

$$G_p = G_f \frac{y_{CH_{4,1}}}{y_{CH_{4,2}}}$$

which, in the present plant data, amounts to about 5 to 6%. This correction has not been made to any of the predicted results shown in Figure 6. The EA-1 model seems slightly better than the EA-2 or EA-3 models for predicting the average axial temperature profile (Figure 6), the adiabatic temperature rise (Figure 8), the exit temperature (Figure 9), and the axial concentration profile (Figure 10). However, the differences are slight among the EA models.

Figure 11 reveals that the EA-2 and EA-3 models predict almost identical parabolic radial temperature profiles at $z = 0.6$. The EA-1 model, because of the highly nonlinear velocity and

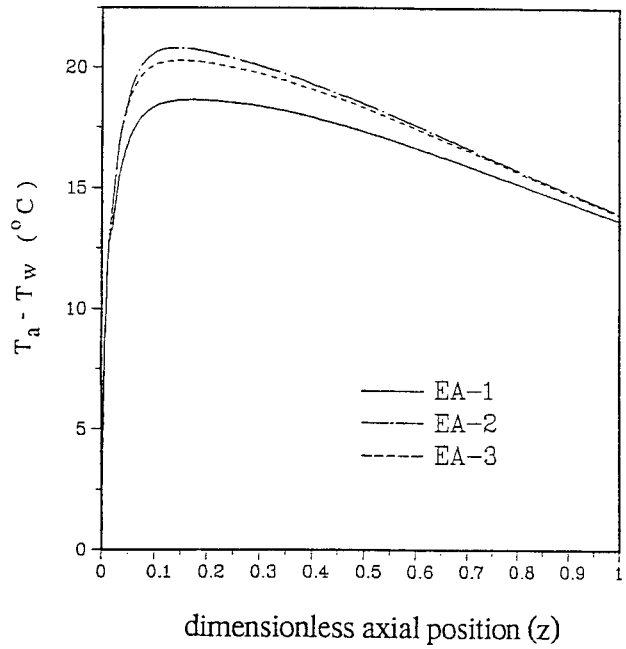

Figure 12. Radial temperature differences by different models.

k_{er} near the wall, predicts a small shoulder near the wall on an otherwise parabolic temperature profile. Although the present plant data do not provide evidence of this shoulder, a shoulder was indicated in the experiments of Leron and Froment (1977).

Finally, the radial temperature difference between the center of the catalyst packing and the wall is predicted in Figure 12 by subtracting the wall and the central temperatures in the cooling section of the reactor (from Figure 7). It is evident that the maximum temperature difference is about 4 to 5°C lower for the EA-1 model than for the other two models.

In contrast to the radial temperature distribution, no appreciable radial concentration difference can be seen throughout the fixed bed (Figure 13). Therefore, a plug-flow, semi-two-dimensional model would appear to be an acceptable choice for the MSS ammonia synthesis reactor.

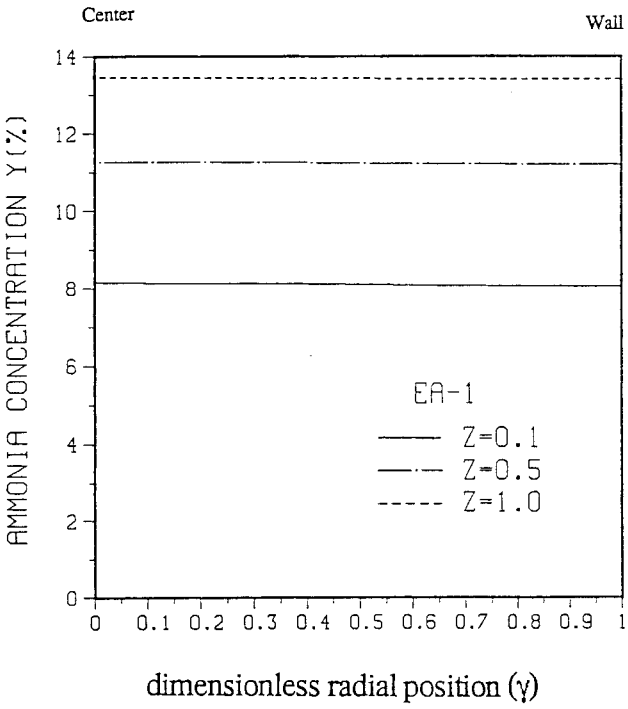

Figure 13. Radial concentration profiles by different models.

Conclusions

Combining the equivalent annular model with the transformed circular model makes it possible to take into consideration radial variations of flow rate and transport properties in modeling an MSS fixed-bed reactor. Comparing predicted axial and radial temperature and concentration distributions with data obtained from an industrial ammonia synthesis reactor demonstrate that the plug flow assumption is well approximated. The approach developed in this article permits one to deal with variations in radial flow and radial transport properties within this complex geometry.

Acknowledgment

The authors would like to gratefully acknowledge the support from the Natural Sciences and Engineering Research Council of Canada.

Notation

c_p, c_f = (reactant, coolant) heat capacity, kJ/kg·K
c = concentration of reactants, products, kmol/m^3
C_p = heat capacity, kJ/kmol·K
d_a = diameter of cooling tubes, m
d_{bed} = diameter of the packed bed
$d_{c.t}$ = diameter of central tube
d_j = constants in Eq. 17
d_p = pellet equivalent diameter, m
d_{riser} = diameter of the side risers
D_m = mean diameter of cooling tube, m
D_w, D_i = outer, inner diameter of cooling tubes, m
D_r = radial mass transfer coefficient, m^2/s
F = cross-sectional area of fixed bed in cooling stage, m^2
F_a = a term in Reaction rate expression, atm$^{-0.5}$
G = mass flow rate, kg/s·m^2
ΔH = heat of reaction, kJ/kmol
k_{er} = effective radial thermal conductivity, kJ/m·s·K
k_o = pre-exponential factor, atm$^{0.5}$/s
K_p = reaction equilibrium constant, atm^{-1}
k_T = reaction rate constant, atm$^{0.5}$/s
k_{wf} = fixed bed-cooling side overall heat transfer coefficient, kJ/m^2·s·K
L = reactor or cooling tube length, m
M_{av} = mean molecular weight of fluid, kg/kmol
m_t = number of cooling tubes
N = radial distance to tube wall measured in pellet diameters; an index in collocation integration
N_z = molar flow rate, kmol/m^2·s
$p(\xi)$ = orthogonal polynomial defined in Eq. 16
r = radial coordinate, m
r_1, r_2 = inner, outer radius of equivalent annular bed, m
R = radius of imaginary fixed bed, m
Rc = dirt coefficient, m^3·s·K/kJ
$r(T, y)$ = reaction rate, kmol/kg cat·s
T, T_{av} = point, average temperature, K
T_c, T_w = coolant, wall temperature, K
T_{in}, T_{exit} = inlet and outlet temperature of reactor, K
T_{inlet} = initial temperature of cooling stage, K
ΔT = adiabatic temperature rise, K
u, u_{av} = linear, average linear empty-tube velocity of reactants, m/h

v, v_{av} = point, average dimensionless velocity, u/u_{av}
w = linear velocity at standard state, m/h
x = axial coordinate, m
X = ammonia produced per 100 kmol feeding stream, kmol
y = mol fraction of resultant
z = dimensionless axial position in fixed bed, x/L

Greek letters

α_1, α_2 = constants in correlation of k_{er} (Eq. 12)
α_f = coolant-wall heat transfer coefficient, kJ/m^2·s·K
α_i = bed-to-wall heat transfer coefficient in one-dimensional model, kJ/m^2·s·K
α_w = heat transfer coefficient between fixed bed and wall in two-dimensional model, kJ/m^2·s·K
a_w°, a_w^* = static fluid-wall, fluid-wall heat transfer coefficient in two-dimensional model, kJ/m^2·s·K
γ = dimensionless radial position $(r_2-r)/(r_2-r_1)$
η = viscosity of fluid
δ = thickness of tube wall, m
ϵ_b, ϵ_w = bulk, near-wall voidage
λ_f = thermal conductivity of gas, kJ/m·s·K
λ_{eo} = fixed bed static effective thermal conductivity, kJ/m·s·K
λ_{tu} = thermal conductivity of tube wall, kJ/m·s·K
ξ_i = radial coordinate of collocation points
σ_k = specific surface of catalyst, m^2/kg
ϕ = angular coordinate in sectional-cross of fixed bed
ω, Ω = coordinate system as in Figure 2
$\Sigma C_{p,i}$ = heat capacity of resultant mixture, kJ/kmol

Dimensionless groups

Pe_m = Peclet (or Bodenstein) number $(d_p u/D_r)$
Pr, Pr_c = Prandtl number in fixed bed, cooling tube $(c_p\eta/\lambda_f)$
Re_p = point Reynolds number, d_pG/η

Subscript

im = transformed circular fixed-bed represented by Eq. 6

Literature Cited

Ahmed, M., and R. W. Fahien, "Tubular Reactor Design. Two-Dimensional Model," *Chem. Eng. Sci.*, **35**, 889 (1980).
Benenati, R. F., and C. B. Brosilow, "Void Fraction Distribution in Beds of Spheres," *AIChE J.*, **8**, 359 (1962).
Fahien, R. W., and I. M. Stankovich, "An Equation for the Velocity Profile in Packed Column," *Chem. Eng. Sci.*, **34**, 1350 (1979).
Finlayson, B. A., "Packed-Bed Reactor Analysis by Orthogonal Collocation Method," *Chem. Eng. Sci.*, **26**, 1081 (1971).
Finlayson, B. A., *The Method of Weighted Residuals and Variational Principles*, Academic Press, London (1972).
Finlayson, B. A., *Nonlinear Analysis in Chemical Engineering*, Academic Press, London (1977).
Hlavacek, V., and J. Votruba, *Chemical Reactor Theory—A Review*, Chap. 6, L. Lapidus and N. R. Amundson, eds., Prentice-Hall, Englewood Cliffs, NJ (1977).
Leron, J. J., and G. F. Froment, "Velocity, Temperature and Conversion Profiles in Fixed-Bed Catalytic Reactors," *Chem. Eng. Sci.*, **32**, 853 (1977).
Li, H. M., M. Eng. Thesis, South China Inst. Technol., Guangzhou, China (1982).
McGreavy, C., E. A. Foumeny and K. H. Javed, "Characterization of Transport Properties for Fixed Beds in terms of Local Bed Structure and Flow Distribution," *Chem. Eng. Sci.*, **41**, 787 (1986).
Rase, H. F., *Chemical Reactor Design for Process Plants*, Vol. 2, p. 61, Wiley, New York (1977).
Roblee, L. H. S., R. M. Baird, and J. W. Tierney, "Radial Porosity Variations in Packed Beds," *AIChE J.*, **4**, 460 (1958).
Smith, J. M., *Chemical Engineering Kinetics*, 3rd ed., McGraw-Hill, New York (1981).
Strelzoff, S., *Technology and Manufacture of Ammonia*, Wiley, New York (1981).
Touzani, A., D. Klvana, and G. Belanger, "A Mathematical Model for the Dehydrogenation of Methylcyclohexane In a Packed-Bed Reactor," *Can. J. Chem. Eng.*, **65**, 56 (1987).
Yagi, S., and D. Kunii, "Studies of Effective Thermal Conductivities in Packed Beds," *AIChE J.*, **3**, 373 (1957).
Yagi, S., and N. Wakao, "Heat and Mass Transfer from Wall to Fluid in Packed Beds," *AIChE J.*, **5**, 79 (1959).

Appendix: Parameters for Ammonia Synthesis Reactor (Li, 1982)

Bed characteristics	
Diameter of fixed bed	438 mm
Number of cooling tubes	40
Diameter of central rising tube	108 mm
Diameter of thermocouple tube	38 mm
Length of adiabatic section	1.1 m
Length of cooling section	4.35 m
Arrangement of cooling tubes	16×2
Equiv. dia. (outer/inner)	0.06624 m/0.016 m
Cross-sectional areas	
Adiabatic section	0.1507 m^2
Cooling section	0.1298 m^2
Volume of catalyst	0.64 m^3
Catalyst	4.0–4.5 mm (spherical)
Bulk porosity	0.42
Bed porosity near wall	0.7
Emissivity of catalyst	0.9
Thermal conductivity of catalyst	1.162×10^{-2} kJ/m·s·K
Dirt coefficient of wall	$Rc=0.6023$ m^3·s·K/kJ
Operation conditions	
Operating pressure	290 atm
Composition of feed	$y_a=0.0292$; $y_{CH_4-Ar}=0.194$; $y_{H_2}/y_{N_2}=3$
Space velocity	8.333 s^{-1}
Modification to rate constant	Corr = 0.6 (in adiabatic section) Corr = 0.6–0.15x (in cooling section)
Kinetic parameters	
Rate constant	7.778 atm$^{-0.5}$s (at 450°C)
Activation energy	−177 kJ/mol (<450°C) −126 kJ/mol (>450°C)

$$Re_p = 2{,}320.78\ v_i \left(v_i = \frac{u_i}{\bar{u}}\right)$$

$$Pr = 0.6254;\ Re = 2.359\times10^5;\ Pr_c = 0.509$$

$$\frac{k_{er}}{\lambda_f} = 8.9192 + 2.038\times10^{-3}G_i$$

$$k_{wf} = \begin{cases} 0.698\ (\text{kJ/m}^2\cdot\text{s}\cdot\text{K}) \text{ for plug flow} \\ 0.604\ (\text{kJ/m}^2\cdot\text{s}\cdot\text{K}) \text{ for variable radial flow rate} \end{cases}$$

Manuscript received July 26, 1989, and revision received Nov. 26, 1990.